Bordes, MDC.; Vicent, M.; Moreno, A.; López, V.; Moreno, R.; Salvador Moya, MD.; Benavente Martínez, R.... (2014). Preparation of feedstocks from nano/submicron-sized TiO2 particles to obtain photocatalytic coatings by atmospheric plasma spraying. Ceramics International. 40(10):16213-16225. doi:10.1016/j.ceramint.2014.07.057.

PREPARATION OF FEEDSTOCKS FROM NANO/SUBMICRON-SIZED TiO_2 PARTICLES TO OBTAIN PHOTOCATALYTIC COATINGS BY ATMOSPHERIC PLASMA SPRAYING

M.C. Bordes[1*], M. Vicent[1], A. Moreno[1], V. López[1], R. Moreno[2], M.D. Salvador[3], R. Benavente[3], E. Sánchez[1]

[(1)] Instituto de Tecnología Cerámica (ITC), Universitat Jaume I, Castellón, E-12006 Castellón, Spain.

[(2)] Instituto de Cerámica y Vidrio (ICV), CSIC, E-28049 Madrid, Spain.

[(3)]Instituto de Tecnología de Materiales (ITM), Universidad Politécnica de Valencia, Camino de Vera s/n, 46022 Valencia, Spain.

Corresponding author: Ms Mari Carmen Bordes

Phone: (+34) 964 64 24 24
Fax: (+34) 964 34 24 25

E-mail: carmen.bordes@itc.uji.es

Abstract

Atmospheric plasma spraying (APS) has been proved useful in obtaining TiO_2 coatings with effective photocatalytic activity. However, the influence of feedstock characteristics on photocatalytic activity has hardly been addressed.

This study was undertaken to prepare TiO_2 photocatalytic coatings by APS from different feedstocks. The feedstocks were obtained by spray drying suspensions of a nano- and a submicron-sized TiO_2 powder, with different solids contents and/or ratios of the nano- to submicron-sized particles. All the resulting powders were fully

characterised to assess their suitability for use in APS processes. Feedstock powders were then deposited on steel coupons by APS using hydrogen or helium as secondary plasma gas. Coating microstructure and phase composition were characterised. Coating photocatalytic activity was determined by measuring the degradation of methylene blue dye in an aqueous solution.

Powder characterisation showed that all feedstocks met plasma spray operation requirements with regard to agglomerate size distribution and density, as well as to powder flowability. Optimum agglomerate density was obtained when a well-balanced mixture of nano- and submicron-sized particles was used.

All coatings displayed a bimodal microstructure with partially melted agglomerates that retained the initial nano- or submicron-sized structure and composition (anatase phase) of the feedstock, surrounded by a fully melted matrix mainly formed by rutile. As expected, coating porosity as well as the amount of partially melted areas depended strongly on plasma spray conditions and on feedstock characteristics.

With regard to photocatalytic activity, a reasonably good fit of a first-order kinetic model to the experimental data was found for all coatings. The kinetic constants obtained displayed higher values than those of a commercial sol-gel coating. The values of these constants were related to feedstock characteristics as well as to plasma spraying conditions on the basis of anatase content. The contribution of other factors to the resulting coating surface is also discussed.

Keywords: D. TiO_2, Photocatalytic activity, Atmospheric plasma spraying, Nanoparticles

1. INTRODUCTION

Titanium dioxide (TiO_2) is known to be one of the best photocatalysts due to its chemical stability, low cost, and lack of toxicity [1]. For photocatalytic applications, titanium dioxide can be used in powder form (slurry) or immobilised in thin layers or coatings obtained by different deposition techniques. TiO_2 powders display outstanding photocatalytic efficiency compared with their coating counterparts due to their higher specific surface area. However, the separation of powder from the liquid used in water treatments and subsequent recycling process is not easy, owing to the nanometre-sized nature of the powder. The engineering of photocatalytic devices and reactors based on supported photocatalytic coatings has consequently drawn much scientific attention in recent years, evidenced by a number of interesting reviews on the subject [2, 3].

Titanium oxide coatings with many applications have been prepared for years by thermal spraying routes due to the hardness, wear and corrosion resistance, and biocompatibility of such coatings [4, 5]. In the last few years, intensive research has shown that thermal spray techniques, especially atmospheric plasma spraying (APS) can also be used to obtain nanostructured TiO_2 coatings with effective photocatalytic activity [6-8]. Obtaining nanostructured coatings by APS requires the reconstitution (granulation) of starting nanopowders into a sprayable size, since nanoparticles can not be deposited directly because of their low mass and poor flowability. Spray drying is the main method used to achieve this goal [9].

Many of these studies have shown the need to preserve as high an amount of anatase phase in the coating as possible, due to its superior photocatalytic performance in comparison with that of rutile [6, 10, 11]. However the factors that control anatase phase distribution in the final layers still remain unclear. Regardless of the nature and composition of the feedstock, a mixture of anatase and rutile is always encountered due to the well-known anatase to rutile transition, which in turn depends, among other factors, on the particle size of the starting phase [12-15]. Many authors have thus observed that the anatase content in the coatings strongly depends on the thermal spray process conditions [6, 12, 13]. More specifically, most of the anatase content in the final coating is assigned to the partially melted or unmelted areas that preserve the nanostructure of the starting feedstock. For this reason, the spraying parameters affecting the energy input of the plasma need to be very carefully adjusted [14].

Although the role of the feedstock on the microstructure and final characteristics of the APS TiO_2 coating is clearly recognised, this has drawn little attention in the literature [12, 16]. Nor has photocatalytic activity been addressed in these studies. In a recent study, the authors reconstituted different nanoparticle suspensions of TiO_2, obtaining sprayable feedstocks that were subsequently deposited by APS, yielding coatings with good photocatalytic activity (similar to that of a commercial sol-gel coating) [17]. In addition, a feedstock comprising nanometre- and submicrometre-sized TiO_2 particles was shown to produce coatings exhibiting slightly higher photocatalytic activity than that of the coatings obtained from feedstocks exclusively made up of nanoparticles. This was a quite interesting finding because it meant that the use of a bimodal distribution of submicron- and nano-sized particles in the precursor suspension for the spray-dried

feedstock could give rise to significant benefits, in particular higher suspension solids content and lower viscosity. This would in turn yield better properties in the resulting feedstock agglomerates, namely denser agglomerates and improved powder flowability. No less importantly, the cost of the feedstock could be significantly reduced by replacing nanoparticles with submicrometre-sized particles.

The present study was undertaken to obtain TiO_2 photocatalytic coatings by APS from different feedstocks. Suspensions were therefore prepared of a nano- and a submicron-sized TiO_2 powder, with different solids contents and/or ratios of the nano- to submicron-sized particles. All suspensions were then reconstituted by spray-drying to obtain suitable plasma torch feedstocks. The feedstocks were applied under different plasma spraying conditions and the photocatalytic activity of the resulting coatings was assessed. The relationship of feedstock characteristics to coating photocatalytic activity is discussed.

2. EXPERIMENTAL PROCEDURE

2.1. Preparation and characterisation of spray-dried feedstocks

Two powders were used as starting materials: a submicron-sized, high purity anatase (Merck, Germany) with a mean particle size of 0.35 µm and specific surface area of 9.5 m^2/g, and a commercial titania nanopowder (AEROXIDE® P25, Degussa-Evonik, Germany). The P25 nanopowder has been widely used in many previous studies on photocatalysis [18]. It contains anatase and rutile phases in a ca. 3:1 ratio with a mean particle size of 20−40 nm [19].

Concentrated suspensions with a total solids contents ranging from 20 vol.% to 40 vol.% were prepared from the above powder samples, which were mixed in proportions of 0 to 100%. The suspension references and characteristics are detailed in Table 1.

Table 1. Characteristics and references of the suspensions prepared as set out in the text

Powder composition (wt%)	Suspension solids content (vol.%)	[(3)]Viscosity (cP)	Density (g/cm^3)	pH
0 Ts[(1)]- 100 Tn[(2)]	30	>5000	1.7	7.4
25 Ts - 75 Tn	30	2000	1.8	7.3
50 Ts - 50 Tn	30	1440	1.8	5.8
75 Ts - 25 Tn	30	1640	1.8	6.8
100 Ts - 0 Tn	30	1110	1.9	6.3
50 Ts - 50 Tn	20	330	1.5	7.3
50 Ts - 50 Tn	40	>5000	2.1	7.1

[(1)] Ts: submicron-sized TiO_2 powder
[(2)] Tn: nanosized TiO_2 powder
[(3)] Determined by torsion wire viscometer (Gallenkamp VHA-205, FISONS, UK**)**

The preparation route for the mixed suspensions is based on procedures developed previously for the preparation of 100%, concentrated nano- or submicron-sized TiO_2 particle suspensions, set out elsewhere [19, 20]. Every suspension was thus prepared by first adding the PAA (polyacrylic dispersant, DURAMAX^{TM} D-3005, Rohm&Haas, USA) required to disperse the nanosized titania (4 wt% with regard to the nanoparticles) and then the PAA required to disperse the submicronic powder (0.3 wt% with regard to the submicron-sized particles). In a second step, nano- and submicron-sized powders were added and the mixture was dispersed first under mechanical agitation (15 min) and then with variable sonication time, which depended on the nanoparticle content in the suspension. Table 1 shows the characteristics of the prepared suspensions.

Spray-dried granules were obtained from all suspensions in a spray dryer (Mobile Minor, Gea Niro, Denmark) with a drying capacity of 7 kg water/h. Spray-drying efficiency was about 40−60%. For the sake of simplicity, the same references were used

for the powder samples as those assigned to the corresponding starting suspensions detailed in Table 1. Granule size distribution was measured by dry sieving. Spray-dried granule bulk density was calculated from powder tapped density as previously reported [21]. Powder flowability was evaluated in terms of the Hausner ratio, determined by dividing tapped density by bulk density. Free-flowing powders present a Hausner ratio < 1.25 [21].

A field-emission environmental scanning electron microscope, FEG-ESEM (QUANTA 200FEG, FEI Company, USA) equipped with an energy-dispersive X-ray spectrometer (EDAX Genesis, USA) was used to analyse feedstock microstructure.

2.2. Preparation and characterisation of the APS coatings

TiO_2 coatings were deposited by APS on metallic substrates (AISI 304) prepared as set out elsewhere [22]. The plasma spray system consisted of a gun (F4-MB, Sulzer Metco, Germany) operated by a robot (IRB 1400, ABB, Switzerland). The main spraying conditions are shown in Table 2, together with an estimate of plasma enthalpy [23]. Deposition was performed using argon as primary gas and hydrogen or helium as secondary gas. Helium gas was used to reduce the heat intensity of the plasma jet. In addition, the following spraying conditions were kept constant throughout all experiments: anode nozzle internal diameter = 6 mm, powder injector diameter = 2 mm, feedstock feed rate = 30 g/min, and scanning step = 4 mm.

Table 2. Main plasma spraying parameters used in the experiments

Secondary plasma gas	**Ar (slpm)**	**H_2 (slpm)**	**He (slpm)**	**$^{(1)}$I (A)**	**$^{(2)}$d (m)**	**$^{(3)}$v (m/s)**	**$^{(4)}\Delta H$ (MJ/kg)**
H_2	38	14	---	600	0.12	1	26 ± 2
He	40	---	20	600	0.12	1	12 ± 1

slpm = standard litre per minute
$^{(1)}$I = arc intensity
$^{(2)}$d = spraying distance
$^{(3)}$v = spraying velocity
$^{(4)}\Delta H$ = enthalpy

A quantitative crystalline phase composition analysis from X-ray diffraction data was conducted based on the Rietveld refinement. The XRD patterns were obtained using a Theta-Theta model diffractometer (D8 Advance, Bruker, Germany) with CuKα radiation (λ = 1.54183 Å). The generator settings were 45 kV and 30 mA. The XRD data were collected in a 2θ of 5−90º with a step width of 0.015º and counting time of 1.2 s/step, by means of a VÅNTEC-1 detector. Details of the Rietveld procedure have been reported elsewhere [17, 24]. Content (wt%) and crystallite size of the crystalline phases (anatase and rutile) were calculated by this method.

Micrographs of cross-sections of the coatings were obtained with a SEM instrument (JSM6300, JEOL, Japan), and coating roughness was measured with a contact profilometer (HOMMELWERKE T8000 (HOMMELWERKE, Germany). The roughness test consisted of obtaining 81 profiles of 4.8-millimetre length until a topographic map of 4.8x4.8mm was created. The cut-off used to obtain the roughness parameter (Ra) after the measurements was 0.8 mm.

Finally, coating porosity and semi-melted particle fractions were evaluated by image analysis (Image pro-Plus, Media Cybernetics, Inc., USA) from ten backscattered electron mode micrographs at 400 magnifications obtained by SEM. [25].

2.3. Assessment of coating photocatalytic activity

Coating photocatalytic activity was assessed by studying the decomposition of a 5 ppm methylene blue (MB) aqueous solution under UV radiation. Irradiation was performed in a chamber using a UV-lamp (λ=370 nm) with an intensity of 2.5 mW/cm^2. The coated samples (disks) were immersed in a glass beaker containing 25 ml of a 5 ppm MB solution. MB solution absorbance was measured at 664 nm wavelength, which is the maximum absorption peak of MB, using a UV-visible spectrometer (Spectro SC, Labomed Inc., USA). In order to allow the MB to be adsorbed on the TiO_2 surface, test pieces were kept in contact with the solution for 24 h in the dark. During this time, MB concentration decreased less than 10 % of the initial concentration. In addition, the dark test showed that the MB concentration hardly varied after 30 min contact of the MB solution with the coating. For this reason, the test pieces were kept in contact with the MB solution for 30 minutes in the dark, prior to irradiation, after which the MB concentration was determined. The samples were then continuously irradiated, a 6 ml volume being withdrawn after 1, 2, 3, 5, 7, 11, and 15 h irradiation to determine the concentration. The solution was stirred before each sampling and the withdrawn test liquid was returned to the solution after UV measurement. A blank sample with no coating was tested to evaluate the influence of UV radiation on the decrease in MB concentration by photolysis.

3. RESULTS AND DISCUSSION

3.1. Characterisation of the feedstocks obtained by spray drying

Figure 1 shows FEGSEM micrographs of the as-spray-dried powders obtained from all suspensions at different magnifications. The typical doughnut-shape morphology of spray-dried agglomerates was observed in certain granules of all powders [25]. In addition, the agglomerates displayed a quite homogeneous, spherical morphology. Most granule sizes ranged from approximately 10 μm to 200 μm. The presence of some satellite-like granules stuck to bigger ones was also observed. It was furthermore noted that sample 50Ts-50Tn (40 vol.%) was made up of more deformed (less spherical) granules with large inner holes inside the coarser granules. This was due to the high viscosity of the sample starting suspension as indicated in Table 1. That is, the higher the viscosity of the spray-drying suspension, the coarser and the more elongated were the resulting granules, as set out elsewhere [26]. Nevertheless, no clear tendencies could be established from the micrographs with regard to starting suspension characteristics and agglomerate size distribution. On the other hand, higher magnification of the solid areas of the agglomerates of all powders revealed that the granules were porous and formed by agglomeration of the individual nano- and submicron-sized particles. Again, differences could be observed between the samples. An increase in submicron-sized particle content in the starting suspensions thus seemed to give rise to a denser particle arrangement in the granules as a result of a better balance between coarse and fine particles.

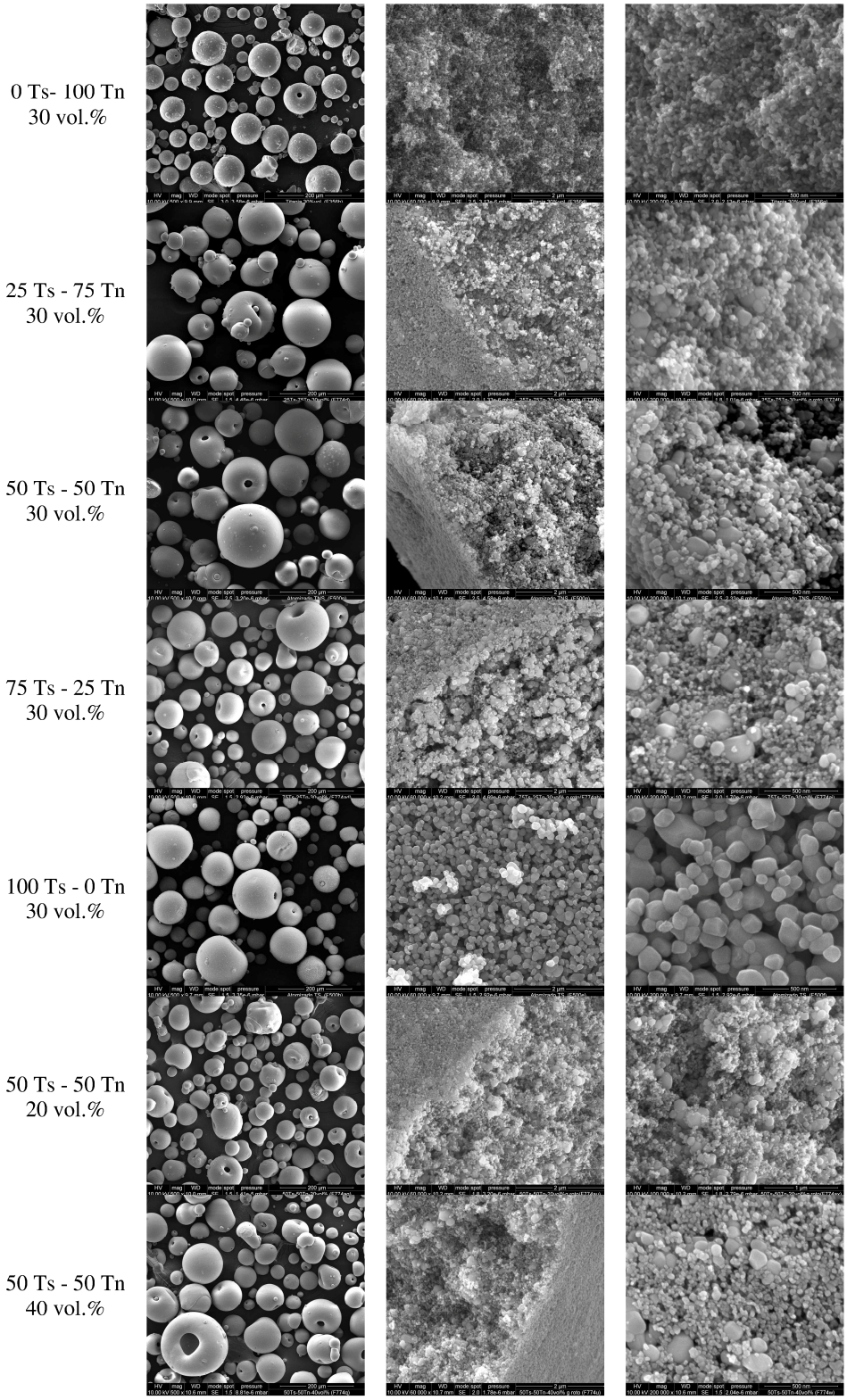

Figure 1. Micrographs of the as-spray-dried powders obtained from all suspensions at different magnifications.

The granule size distributions of the two series of samples, measured by dry sieving, are shown in Figure 2. It should be noted that the minimum mesh aperture available for dry sieving was 45 μm. As may be observed, all powders exhibited similar, quite narrow granule size distributions except sample 0Ts-100Tn (100% nanoparticle content), in which the distribution shifted to coarser granule sizes with practically no granules below 60 μm. This shift was caused by the high viscosity of the sample starting suspension (see Table 1) [26]. It is generally recognised that thermal spray powders should adopt agglomerate size distributions ranging from 10 to 100 μm so that the feedstock can flow and melt during the plasma spray operation [9]. In this case, all the feedstocks contained coarser agglomerates, mainly within the 125-200 μm range due to the relatively high viscosity of the suspensions used to spray-dry. Nevertheless, according to previous research by the authors this coarser agglomerate fraction does not affect the feedstock sprayability in the plasma or the microstructure and final properties of the coatings [17, 25].

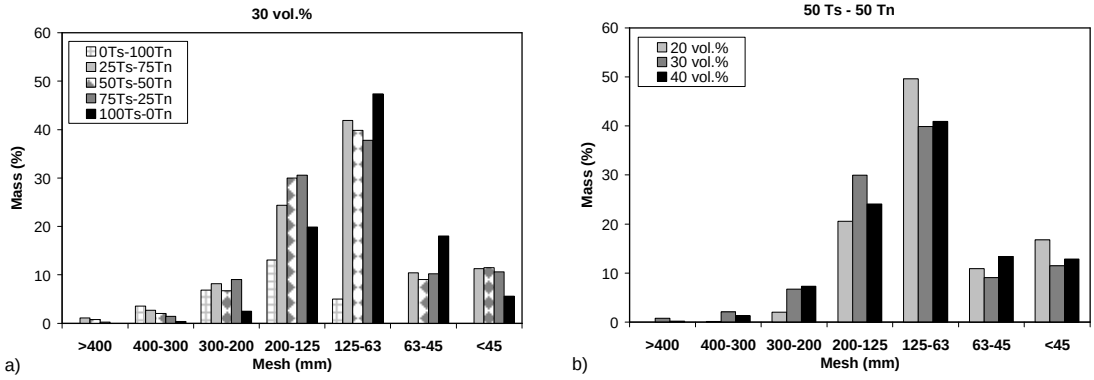

Figure 2. Granule size distributions measured by dry sieving: a) samples in which the ratio of the nano- to submicron-sized particles was changed; and b) samples in which the solids content of the starting suspensions was varied.

Two other properties of interest in spray-dried powder feedstock for plasma spraying are plotted in Figure 3: the Hausner ratio, which is related to powder flowability, and

agglomerate bulk density, which is directly related to powder weight. According to the literature [9], relatively dense (higher than 1000 kg/m^3 apparent density) and free-flowing agglomerates are required for plasma torch feed. In general, all samples exhibited adequate characteristics for use as APS powders. However, certain differences could again be observed among the samples. With regard to agglomerate bulk density, raising submicron-sized particle content in the starting suspension led to significant enhancement of agglomerate density as a result of the better packing efficiency of the resulting bimodal (nano- and submicron-sized) particle size distribution (Figure 3a). Studies based on particle packing models have shown that the maximum packing density for bimodal distributions of spherical particles is found in mixtures comprising 60−70 vol.% of coarse particles and 30−40 vol.% of finer particles, the latter filling the interstices created by the coarser ones [27]. On the other hand, as expected, raising starting suspension solids content gave rise to denser agglomerates (Figure 3b). Both findings confirmed the micrograph observations set out above. With regard to powder flowability, all samples could be considered free-flowing powders [28]. The small differences observed in sample Hausner ratios did not allow correlations between agglomerate characteristics and these ratios to be established (Figure 3c,d). In short, all analysed feedstocks met plasma spraying requirements with regard to agglomerate size distribution and density, as well as to powder flowability.

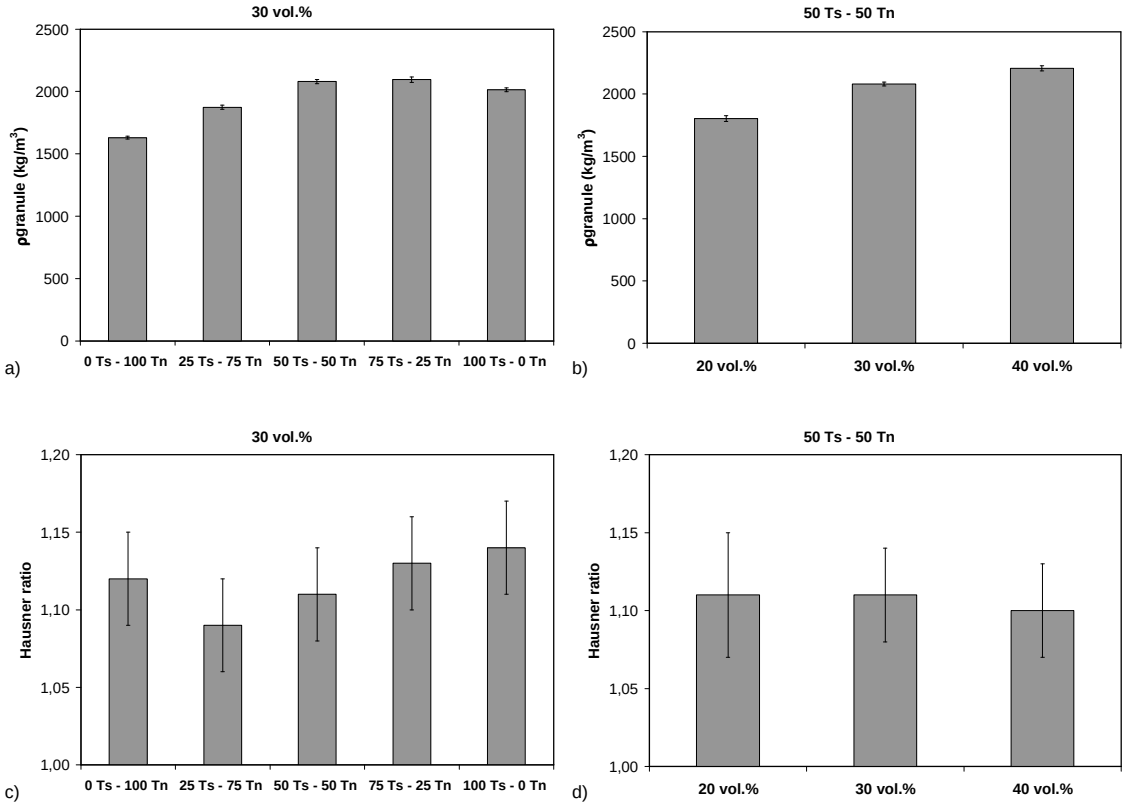

Figure 3. Variation of agglomerate bulk density and Hausner ratio respectively for: a) and c) powders in which the ratio of the nano- to submicron-sized particles was changed; and b) and d) powders in which the solids content of the starting suspension was varied.

3.2 Coating microstructure and phase distribution

As noted above, all powders were previously dry sieved at 200 μm mesh aperture to remove very coarse agglomerates. The resulting powders were then deposited by plasma spray under two different spraying conditions, i.e. using either hydrogen or helium as plasma secondary gas (Table 2). A total of 14 different types of coatings were thus plasma sprayed. The coating samples were assigned the same references as those used for their powder counterparts (Table 1). For the sake of simplicity, Figure 4 shows SEM micrographs of only 4 coatings obtained with H_2 as secondary plasma gas. No significant differences were observed for the other coatings obtained with H_2 and He. Micrographs of this type of coatings obtained from He can be observed in previous

research [17]. The coatings displayed the typical microstructure of TiO_2 layers deposited from nanostructured or submicron-sized particle feedstock reported in the literature, according to which these coating microstructures basically comprise two clearly differentiated zones, yielding a bimodal structure [10, 16, 17, 29]. One coating region, which was completely melted, consisted mainly of an amorphous titania matrix with recrystallised nanometre-sized grains of rutile. Rietveld analysis revealed that the rutile crystallite size in the coatings ranged from 33 nm (coating 75Ts-25Tn obtained in H_2) to 131 nm (coating 100Ts-0Tn obtained in He). The other coating region, which was only partially melted, largely retained the microstructure of a slightly sintered or non-sintered starting powder. This microstructure was therefore principally made up of nanometre- to submicron-sized grains of anatase. On the other hand the amount of unmelted zones appeared to increase as submicron-sized particle content in the feedstock rose. Figure 5 shows higher magnification micrographs of coatings 0Ts-100Tn (100% nanoparticles in the powder feed) and 100Ts-0Tn (100% submicron-sized particles in the powder feed). As expected, the unmelted areas consisted basically of nanoparticles or submicron-sized particles that had undergone some degree of sintering. Thus, under given plasma spray conditions (plasma energy), the amount and size of the particles inside these unmelted zones obviously depended not only on the size of the particles making up the feedstock agglomerates (nanoparticles or submicron-sized particles), but also on other feedstock characteristics such as agglomerate size and density. The difficulty in analysing the structure of these unmelted zones made it hard to try to establish correlations between feedstock characteristics and unmelted zone microstructure.

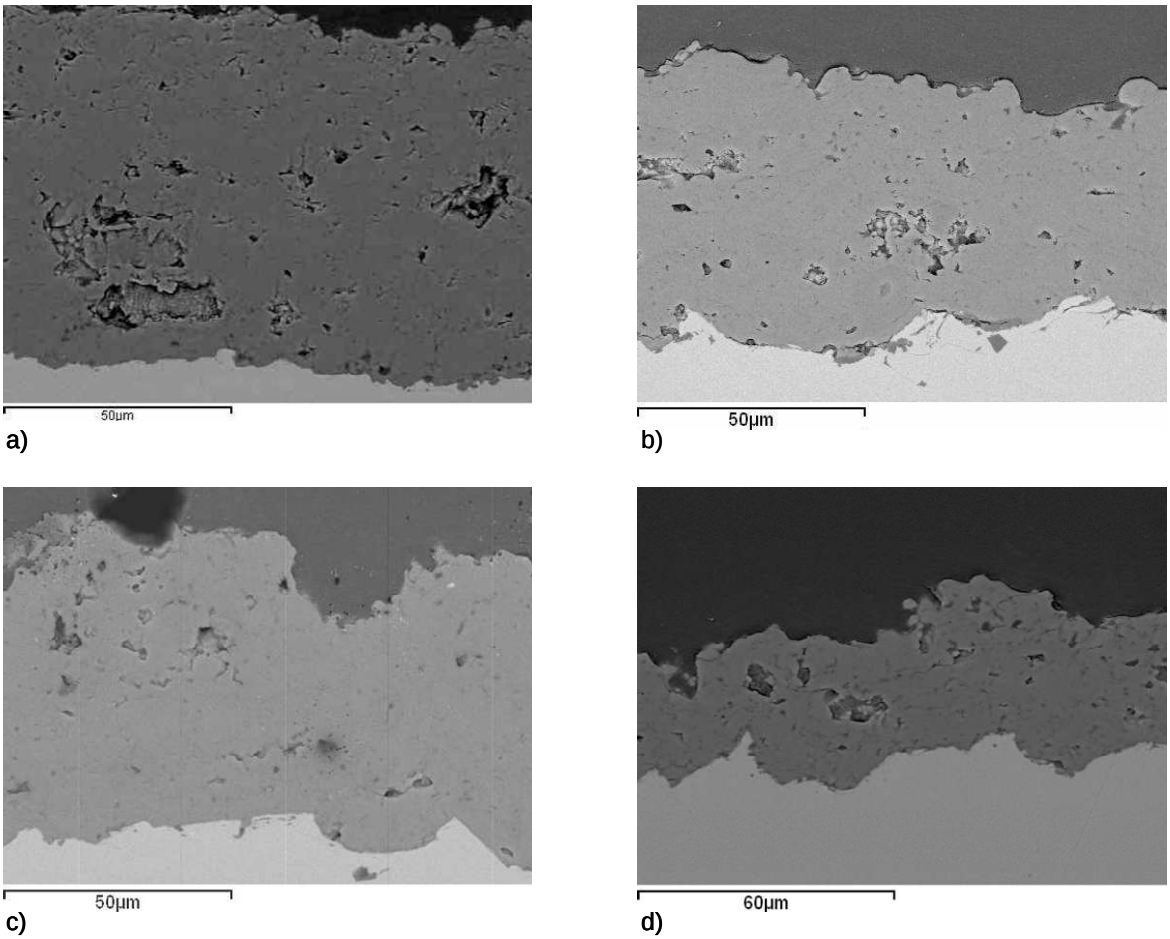

Figure 4. SEM micrographs of the coatings obtained using H_2 as plasma gas from: a) 0Ts-100Tn (100% nanoparticle feedstock, 30 vol.%); b) 50Ts-50Tn (50% submicron-sized particle and 50% nanoparticle feedstock, 30 vol.%); c) 100Ts-0Tn (100% submicron-sized particle feedstock, 30 vol.%); and d) 50Ts-50Tn (50% submicron-sized particle and 50% nanoparticle feedstock, 40 vol.%) powders.

Finally, with regard to porosity, all coatings were porous, exhibiting the typical lamellar structure of plasma sprayed coatings. Smaller pores were thus located within individual lamellae and larger pores were found along the interlamellar boundaries [30].

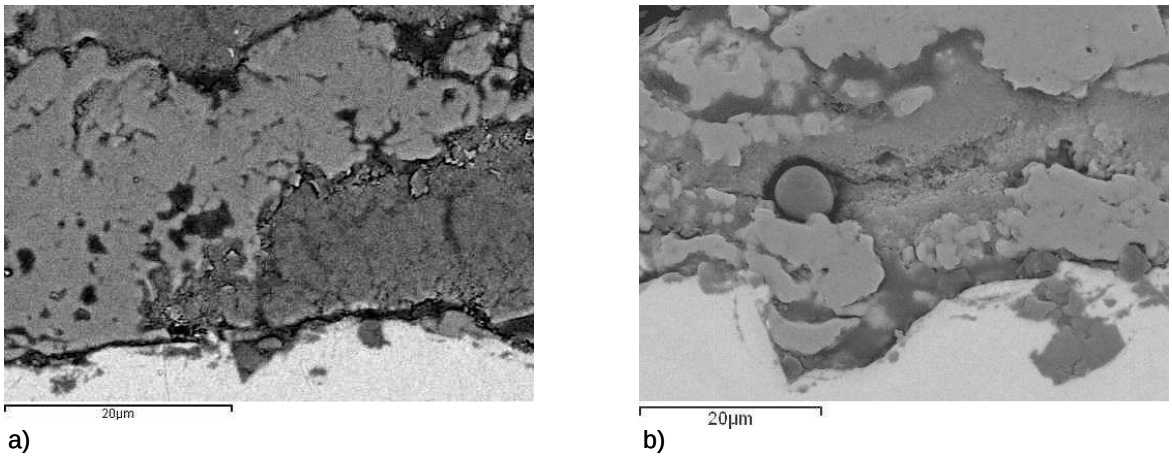

Figure 5. Higher magnification SEM micrographs of the coatings obtained from: a) 0Ts-100Tn (100% nanoparticle feedstock); and b) 100Ts-0Tn (100% submicron-sized particle feedstock) powders with He as plasma gas.

In view of the above, the total porosity of the coatings, as well as the extent of the semi-melted areas, was estimated by image analysis at 400 magnifications using a procedure set out elsewhere [25]. The porosity and semi-melted area data for all coatings are represented as histogram plots in Figure 6. This figure (left) shows that the porosity of all coatings displayed the values typically found in APS coatings. In general, porosity increases when helium gas is used owing to the lower plasma heat input [6, 16, 29]. However, unlike a previous study on nanostructured feedstocks [17], the effect of feedstock characteristics on coating porosity was also observed. It was thus noted that introducing submicron-sized particles in a nanostructured powder led to less reactive plasma torch feed, resulting in coatings with higher porosity. However, there was no direct relationship between submicron-sized particle content and porosity. This was because the increase in submicron-sized particles gave rise to denser agglomerates, contributing to lower coating porosity. With regard to the effect of starting suspension solids content on the porosity of the coatings obtained with the resulting feedstocks, the data suggest that coating porosity decreased as solids content increased, owing to the

higher density of the agglomerates obtained from the suspension with the higher solids content, as set out above. This confirms the results of a previous study on nanostructured Al_2O_3−TiO_2 coatings [25]. However, sample 50Ts-50Tn (40 vol.%) departed from this trend, probably because of the high viscosity of the 40 vol.% suspension, which made it difficult to properly perform the spray-drying operation. In regard to the unmelted or partially melted areas, as expected, the use of helium as plasma gas led to a significant increase in these areas, owing to the lower plasma heat input provided by helium compared to that of hydrogen. In addition, when He gas was used, the extent of the semi-melted areas also rose significantly as the submicron-sized particle content in the feedstock increased. This confirmed the conclusions drawn from the micrographs shown in Fig. 4. In contrast, the extent of the unmelted areas in the coating displayed no clear trend with the feedstocks obtained from suspensions with different solids contents. This was probably because, as previously reported, porous nanozones are produced by two simultaneous, albeit antagonistic effects: the melting of agglomerates and the infiltration of the molten shell into the inner porosity of the agglomerates [5]. However, the effect of agglomerate porosity on the evolution of both phenomena is far from being proved. It may be noted that, on varying plasma spray conditions as well as feedstock characteristics, the extent of the unmelted areas went from 5% to almost 50%, as shown in Fig. 6.

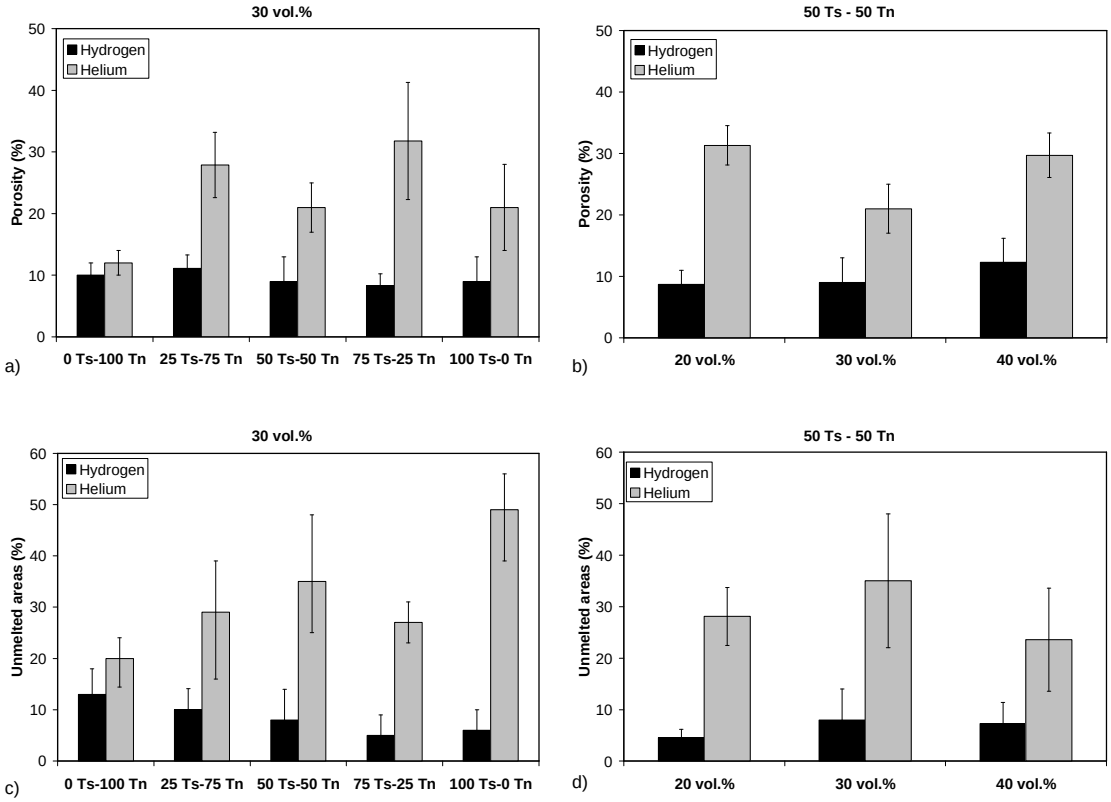

Figure 6. Porosity and semi-melted areas respectively for: a) and c) coatings obtained from samples in which the ratio of the nano- to submicron-sized particles was changed; and b) and d) coatings obtained from samples in which the solids content was varied.

With regard to the phases present in the final coatings, in all cases the coatings were mainly made up of variable amounts of rutile and anatase phases, with minor contents of Magneli phases as previously reported [31]. By way of illustration, Figure 7 shows the XRD patterns of two extreme samples: the coating obtained from 0Ts-100Tn feedstock (100% nanosized particles) and the coating obtained from 100Ts-0Tn feedstock (100% submicron-sized particles) deposited with hydrogen and helium. In both spectra, the coatings obtained with H_2 exhibited a less crystalline pattern than those deposited with He.

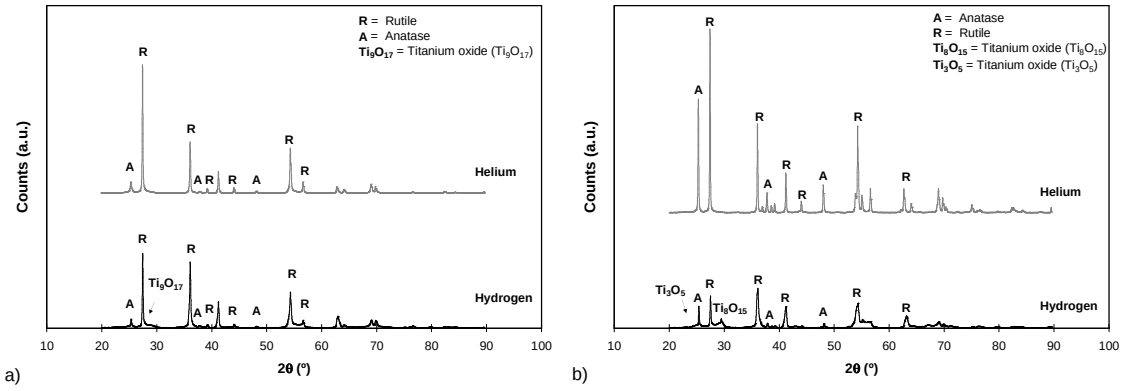

Figure 7. XRD patterns of the coatings obtained in hydrogen and helium from: a) 0Ts-100Tn feedstock (100% nanosized particles); and b) 100Ts-0Tn feedstock (100% submicron-sized particles).

Using the Rietveld method, it was found that the main crystalline phase present in the coatings was rutile, ranging from 18 to 58 wt%. However, anatase is the most important phase for photocatalytic application. The calculated anatase content in all coatings is plotted in Figure 8. The coatings obtained with helium exhibited a much higher anatase phase content, regardless of the feedstock used [6, 29]. Regarding the influence of the starting powder, the two plots in Fig. 8 are very similar to the equivalent plots in Fig. 6, in particular for the coatings obtained with He, in which the extent of the unmelted areas and the anatase content were much higher. This similarity indicates that most of the anatase content in the coating was related to the unmelted areas, in which the starting anatase content was preserved without undergoing the anatase−rutile transition [15, 32]. These findings are in good agreement with the results reported in the literature [6, 10]. In this respect, most of the research on TiO_2 APS coatings has demonstrated that the metastable anatase phase in these coatings is almost exclusively related to the presence of unmelted starting agglomerates. In fact, some authors [12] have shown there was a good linear fit between the areas of the partially melted or unmelted zones in the coating with the anatase content.

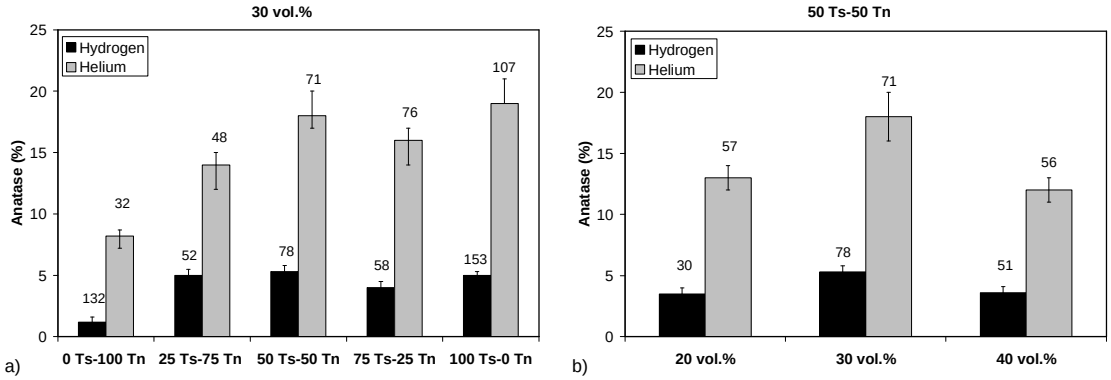

Figure 8. Anatase content in the coatings calculated by the Rietveld method for: a) feedstocks in which the ratio of the nano- to submicron-sized particles was changed; and b) feedstocks in which the solids content was varied.

Nevertheless, although other authors [16, 33] have showed that some anatase is encountered even when the feeding powder is purely rutile, the resulting anatase content in the coating was always much lower than that obtained when anatase powder feedstocks were used. Thus, when the anatase content in the coatings was plotted versus the extent of the unmelted areas (Figure 9), although data scattering is observed, the plot suggests that the anatase particles preserved in the unmelted areas provided the most relevant contribution to the anatase content in the coating.

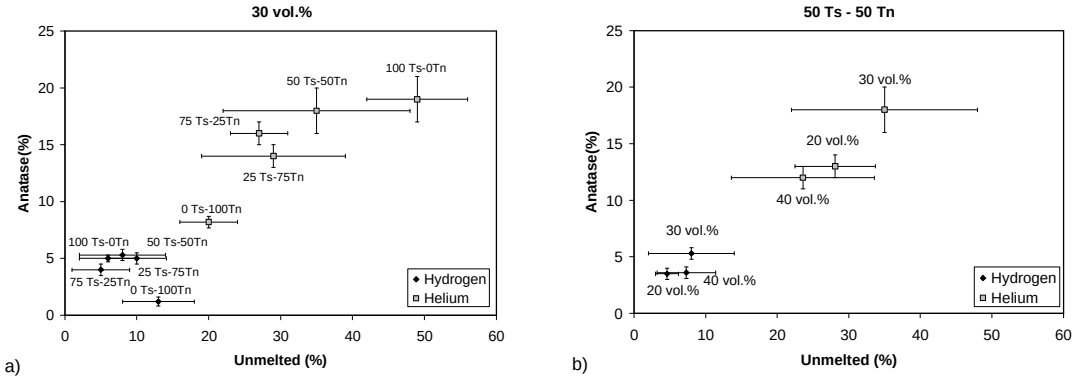

Figure 9. Relationship between anatase content and extent of the unmelted areas for all coatings: a) feedstocks in which the ratio of the nano- to submicron-sized particles was changed; and b) feedstocks in which the solids content of the starting suspensions was varied.

The anatase crystallite size (in nm), calculated by the Rietveld method, is also detailed on the top of each histogram in Fig. 8. In general, when less energetic conditions were used (He gas) during plasma deposition, there was a good relationship between the crystallite size of the anatase phase and the ratio of the nano- to submicron-sized particles in the feedstocks. That is, the higher the amount of submicron-sized particles, the coarser was the crystallite size. This again confirmed that most of the anatase phase present in the coating was related to the preserved, partially melted areas. On the other hand, anatase crystallite size was observed to increase in most coatings when H_2 was used as secondary gas instead of He. Hydrogen enhanced heat transfer from the plasma to the feed, raising particle temperature and heightening the sintering effect. This was particularly noticeable in the coating obtained from the 0Ts-100Tn feedstock (100% nanoparticles), in which the enhancement of crystallite size on switching from He to H_2 was very pronounced. This was because the plasma energy was sufficiently large to significantly reduce the extent of unmelted zones and to promote nanoparticle growth by sintering.

Finally, roughness (Ra parameter) was measured of all coatings. Small differences were observed between the coatings. The Ra values ranged from 3.5 ± 0.3 μm (coating 0Ts-100Tn) to 5.7 ± 0.4 μm (coating 100Ts-0Tn).

3.3 Assessment of coating photocatalytic activity

Coating photocatalytic activity was determined by measuring the degradation of methylene blue (MB) dye in an aqueous solution. For the sake of simplicity, Fig. 10 shows the variation in MB concentration with irradiation time for the solutions in

contact with only three representative coating samples: 0Ts-100Tn, 100Ts-0Tn, and 50Ts-50Tn (30 vol.%) together with a blank substrate.

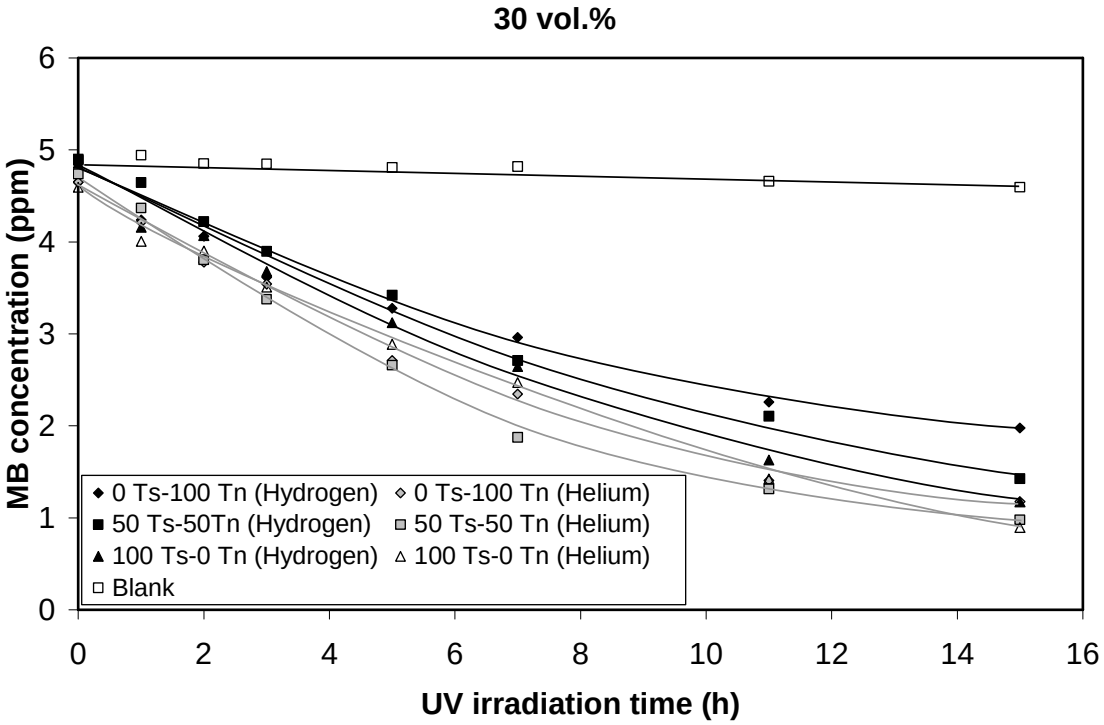

Figure 10. Variation of MB concentration with irradiation time for the solutions in contact with three representative coating samples: 0Ts-100Tn (100% nanoparticle feedstock); 100Ts-0Tn (100% submicron-sized particle feedstock); and 50Ts-50Tn (30 vol.%) together with a blank substrate.

As can be seen, there were clear differences in the MB concentrations at each irradiation time. The coated samples exhibited a pronounced decrease in MB concentration, whereas the blank substrate displayed no significant degradation after UV irradiation. This confirmed the photocatalytic activity of the tested coatings. Similar results were obtained for all coatings, regardless of the feedstock used.

The variation in MB concentration with time may be plotted using a first-order kinetic equation, as previously reported [11]. The constant of photocatalytic activity k (h^{-1}) can then be calculated from the kinetic equation fit. A higher value of k means a faster degradation rate of the organic molecule of MB, i.e. higher photocatalytic activity.

The rate constants determined from the kinetic model for all coatings are shown as histogram plots in Figure 11. The correlation coefficients of the kinetic equation fit are included on the top of each bar. The correlation coefficients for all samples but one were higher than 0.985, indicating reasonably good fit of the experimental data to the kinetic model. A similar fit was found by the authors in previous research [11, 17]. To better understand the magnitude of the photocatalytic effect of these coatings, it may be noted that a sol-gel, TiO_2 commercial photocatalytic coating exhibited a rate constant of $5.98 \pm 0.95 \cdot 10^{-2}$ h^{-1} [17].

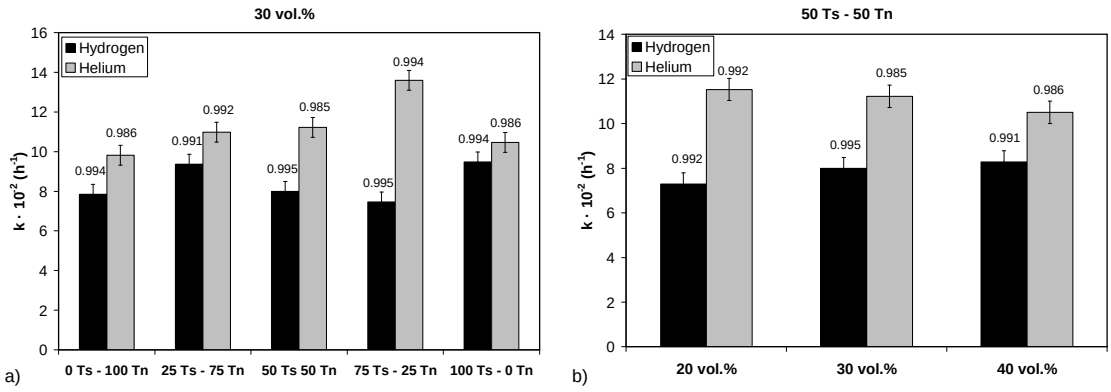

Figure 11. Rate constants determined from the kinetic model for coatings obtained from: a) feedstocks in which the ratio of the nano- to submicron-sized particles was changed; and b) feedstocks in which the solids content of the starting suspensions was varied.

As may be observed in Fig. 11, in general, the photocatalytic effect represented by the k values of the coatings obtained in this study was higher than that of the commercial

product. In fact, certain k values doubled that of the commercial layer. However, any direct comparison between sol-gel and APS coatings should be performed with great caution because the microstructure and, more importantly, the thickness of these types of layers are quite different. On the other hand, as Fig. 8 led to expect, the coatings obtained with He displayed higher photocatalytic activity than those projected with H_2, owing to the higher preserved anatase phase content. The coatings deposited from feedstocks made up of mixtures of nanometric and submicronic particles therefore exhibited greater photocatalytic activity than that of the coating obtained from the 0Ts-100Tn feedstock. In fact, except sample 100Ts-0Tn (which did not follow the expected trend), when the amount of submicron-sized particles in the feedstock increased, the photocatalytic activity of the resulting coatings rose. This confirmed previous research in which the photocatalytic activity of different nanostructured feedstocks and one nano- and submicron-sized TiO_2 feedstock was first compared [17]. Finally, the photocatalytic activity of the coatings obtained from the feedstocks in which the suspension solids content was varied (coatings T2, T20, and T40), plotted in Fig. 11b, was very similar in the three cases, without presenting any clear trend, though the preserved anatase phase content in the coatings exhibited some differences.

The value of k versus anatase content of all the obtained coatings is plotted in Figure 12. To better understand the plot, the composition of the sample in terms of nano/submicron-sized particles or the vol.% concentration indicated in Table 1 was left as a reference of the different samples. As can be seen, although the data exhibit significant scattering, the photocatalytic activity of the coatings for the MB conversion displayed some correlation with the anatase phase content. This is consistent with a

substantial part of relevant publications [10, 13, 29]. Consequently, higher anatase phase content led to faster degradation of MB. On the other hand, the fact that higher photocatalytic activity was obtained for feedstocks comprising mixtures of nano- and submicron-sized titania powders confirmed that anatase content played a greater role than anatase crystallite size, provided the sufficiently fine anatase phase crystals (nanometre- or submicrometre-sized) [13, 34]. In addition, Figure 12 evidences that coatings containing nearly 0% anatase also exhibited non-negligible photocatalytic activity. In fact, other authors have reported photocatalytic activity of plasma sprayed titania coatings mainly made up of rutile [7, 35], although no justification for this behaviour has been put forward.

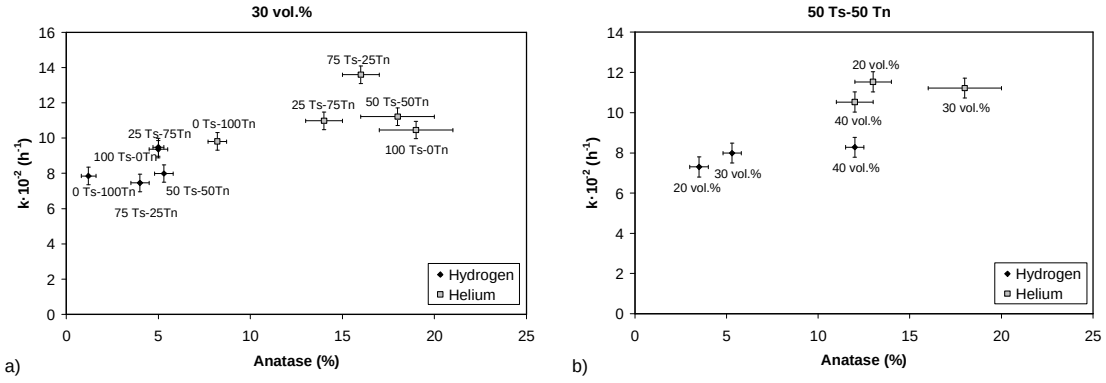

Figure 12. k values versus anatase content for all obtained coatings. Note that the composition (nano/submicron-sized particles) or the vol.% concentration of the starting suspensions for feedstock samples indicated in Table 1 was left as a reference of the different coatings.

The lack of a unique correlation between photocatalytic activity and anatase content is far from being unexpected. In a recent review of some misconceptions of photocatalysis research, Ohtani states that photocatalytic activity cannot be explained by just one variable or parameter of the layer while it is still unclear which properties of the photocatalyst are significant and how many parameters are required for a description of photocatalytic activity [36].

The recent research on photocatalytic TiO_2 coatings obtained by different plasma spraying methods appears to be consistent with this last statement. This suggests that photocatalytic activity arises from a combination of structural and chemical parameters. Ctibor et al. found that the best plasma sprayed TiO_2 coating in terms of photocatalytic activity exhibited higher porosity, medium roughness, some –OH groups on the surface and more surprisingly interstitial nitrogen atoms coming from the ambient air that surrounded the plasma [7]. In this same sense, a research on the effect of H_2 plasma gas on the presence of these –OH groups could be addressed. Nevertheless, in other studies, porosity or surface roughness has been also proved not to significantly influence photocatalytic activity at least with regard to the porosity and roughness variations found in plasma spray coatings [11, 17]. In fact, the present research has shown the secondary role of these structural parameters in comparison with anatase content. Toma et al. [37] also highlight the role played by the hydroxylation state of the coating surface in enhancing photocatalytic performance. Finally, other authors state that, since the plasma used for thermal spraying is a strong UV-light source, photogenerated holes can yield the formation of surface-bound hydroxyl groups, which are oxidising agents and play important roles in photocatalytic reactions [38]. However, it should be noted that all the research mentioned has been carried out on the basis of a wide variety of model compounds (liquids and gases) and methods, which makes it very difficult to draw clear conclusions. Consequently, as the TiO_2 photocatalytic reaction is a surface reaction, the characterisation of surface states in regard to the chemisorbed species, as well as to the presence of vacancies and impurities, should be addressed. Further research is therefore required to clarify the role of the coating surface in the photocatalytic activity of plasma spray TiO_2 coatings. Research to characterise the surface by XPS, Raman and IR

spectroscopy, as well as the determination of the band gap by UV-visible spectroscopy, is now in progress for certain selected coatings.

4. CONCLUSIONS

A nanostructured and a submicron-sized TiO_2 powder were used to prepare feedstocks for deposition by atmospheric plasma spraying. The feedstocks were obtained from concentrated suspensions in which the solids contents and/or the ratios of the nano- to submicron-sized particles were conveniently varied. The suspensions were then spray-dried to obtain APS feedstocks. These powders were characterised in terms of plasma spraying requirements.

All powders met the recommendations set out in the literature with regard to agglomerate size and density as well as to powder flowability. The feedstock obtained from the 100% nanoparticle suspension exhibited a larger amount of finer (<45 μm) agglomerate size fraction. Higher solids content in the starting suspension gave rise to denser agglomerates. Maximum agglomerate density was obtained from binary mixtures of nano- and submicron-sized particles when the mixture approached the optimum volume ratio of 60 coarse (submicron-sized)/40 fine (nanosized) particles of the ideal (spherical) particle packing models.

Regardless of the feedstock used, all coatings displayed a bimodal microstructure with partially melted agglomerates that retained the initial nano- or submicron-sized structure of the feedstock surrounded by a fully melted matrix. As expected, coating porosity and the amount of partially melted areas increased when helium was used as plasma

secondary gas instead of hydrogen, owing to the lower plasma heat input. The increased proportion of submicron-sized particles in the feedstock also contributed significantly to the rise in unmelted areas, which reached up to almost 50% of the total coating cross-section. In all cases, the coatings were mainly made up of rutile (18−58 wt%) and anatase (1.2−19 wt%), the preserved anatase particles in the unmelted areas being the most relevant contribution to the anatase content in the final coatings. In addition, anatase crystallite size increased when H_2 was used as plasma gas instead of He, owing to the higher sintering effect provided by the hydrogen plasma.

The degradation of methylene blue (MB) dye in an aqueous solution was used as a method to assess the photocatalytic activity of the coatings. A reasonably good fit of a first-order kinetic model to experimental data was found for all coatings. The kinetic constants obtained displayed higher values than those of a commercial sol-gel coating. When submicron-sized particle content increased, photocatalytic activity was enhanced, owing to the greater amount of anatase phase preserved in the unmelted areas of the coatings. Although a direct correlation was found between anatase content and photocatalytic activity, the significant data scattering observed indicates the contribution of other factors apart from coating anatase content, in particular those related to the coating surface.

Acknowledgements

This work has been supported by the Spanish Ministry of Economy and Competitiveness (project MAT2012-38364-C03) and co-funded by the ERDF

(European Regional Development Fund), as well as by University Jaume I of Castellon (P1·1B2013-69).

REFERENCES

1. M.A. Henderson, A surface science perspective on TiO_2 photocatalysis, Surface Science Reports 66 (2011) 185-297.
2. S. Malato, P. Fernández-Ibáñez, M.I. Maldonado, J. Blanco, W. Gernjak, Decontamination and disinfection of water by solar photocatalysis: Recent overview and trends, Catalalysis Today 147 (2009) 1-59.
3. M. N. Chong, B. Jin, C.W.K. Chow, C. Saint, Recent developments in photocatalytic water treatment technology: A review, Water Research 44 (2010) 2997-3027.
4. R. B. Heimann, Applications of plasma-sprayed ceramic coatings, Key Engineering Materials 122-124 (1996) 399-442.
5. R.S. Lima, B.R. Marple, Thermal spray coatings engineered from nanostructured ceramic agglomerated powders for structural, thermal barrier and biomedical applications: A Review, Journal of Thermal Spray Technology 16 (2007) 40-63.
6. L. Toma, N. Keller, G. Bertrand, D. Klein, C. Coddet, Elaboration and characterization of environmental properties of TiO_2 plasma sprayed coatings, International Journal of Photoenergy 5 (2003) 141-145.
7. P. Ctibor, V. Stengl, I. Pís, T. Zahoranová, V. Nehasil, Plasma sprayed TiO_2: The influence of Power of an electric supply on relations among stoichiometry, surface state and photocatalytic decomposition of acetone, Ceramics International 38 (2012) 3453-3458.
8. M. Bozorgtabar, M. Rahimipour, M. Salehi, M. Jafarpour, Structure and photocatalytic activity of TiO_2 coatings deposited by atmospheric plasma spraying, Surface and Coatings Technology 205 (2011) S229-S231.
9. P. Fauchais, G. Montavon, R.S. Lima, B.R. Marple, Engineering a new class of thermal spray nano-based microstructures from agglomerated nanostructured particles, suspensions and solutions: an invited review, Journal of Physics D: Applied Physics 44 (2011) 093001 http://dx.doi.org/10.1088/0022-3727/44/9/093001.
10. F.L. Toma, L.M. Berger, D. Jaquet, D. Wicky, I. Villaluenga, Y.R. de Miguel, J.S. Lindeløv, Comparative study on the photocatalytic behaviour of titanium oxide thermal sprayed coatings from powders and suspensions, Surface and Coatings Technology 203 (2009) 2150-2156.
11. E. Bannier, G. Darut, E. Sánchez, A. Denoirjean, M.C. Bordes, M.D. Salvador, E. Rayón, H. Ageorges, Microstructure and photocatalytic activity of suspension plasma sprayed TiO_2 coatings, Surface and Coatings Technology 206 (2011) 378-386.
12. G. Bertrand, N. Berger-Keller, C. Meunier, C. Coddet, Evaluation of metastable phase and microhardness on plasma sprayed titania coatings, Surface and Coatings Technology 200 (2006) 5013-5019.

13. Ch. Lee, H. Choi, Ch. Lee, H. Kim, Photocatalytic properties of nano-structured TiO_2 plasma prayed coatings, Surface and Coatings Technology 173 (2003) 192-200.
14. J.R. Colmenares-Angulo, V. Cannillo, L. Lusvarghi, A. Sola, S. Sampath, Role of process type and process conditions on phase content and physical properties of thermal sprayed coatings, Journal of Materials Science 44 (2009) 2276-2287.
15. G. Mauer, A. Guignard, R. Vassen, Plasma spraying of efficient photoactive TiO_2 coatings, Surface and Coatings Technology 220 (2013) 40-43.
16. N. Berger-Keller, G. Bertrand, C. Filiatre, C. Meunier, C. Coddet, Microstructure of plasma-sprayed titania coatings deposited from spray-dried powder, Surface and Coatings Technology 168 (2003) 281-290.
17. M.C. Bordes, M. Vicent, A. Moreno, R. Moreno, A. Borrell, M.D. Salvador, E. Sánchez, Microstructure and photocatalytic activity of APS coatings obtained from different TiO_2 nanopowders, Surface and Coatings Technology 220 (2013) 179-86.
18. T. Ohno, K. Sarukawa, K. Tokieda, M. Matsumura, Morphology of a TiO_2 photocatalyst (Degussa, P-25) consisting of anatase and rutile crystalline phases, Journal of Catalysis 203 (2001) 82-86.
19. M. Vicent, E. Sánchez, I. Santacruz, R. Moreno, Dispersion of TiO_2 nanopowders to obtain homogeneous nanostructured granules by spray-drying, Journal of the European Ceramic Society 31 (2011) 1413-1419.
20. T. Molina, M. Vicent, E. Sánchez, R. Moreno, Dispersion and reaction sintering of alumina-titania mixtures, Materials Research Bulletin 47 (2012) 2469–2474.
21. J.L. Amorós, A. Blasco, J.E. Enrique, F. Negre, Características de polvos cerámicos para prensado (Characteristics of ceramic powders for pressing), Boletín de la Sociedad Española de Cerâmica y Vidrio 26 (1987) 31-37.
22. E. Sánchez, E. Bannier, V. Cantavella, M.D. Salvador, E. Klyastkina, J. Morgiel, J. Grzonka, A.R. Boccaccini, Deposition of Al_2O_3-TiO_2 nanostructured powders by atmospheric plasma spraying, Journal of Thermal Spray Technology 17 (2008) 329-337.
23. C. Delbos, J. Fazilleau, V. Rat, J F. Coudert, P. Fauchais, B. Pateyron, Phenomena involved in suspension plasma spraying part 2: Zirconia particle treatment and coating formation, Plasma Chemistry and Plasma Processing. 26 (2006) 371–391.
24. R. A. Young (Ed.), The Rietveld method, University Press, Oxford, 1996.
25. E. Sánchez, A. Moreno, M. Vicent, M.D. Salvador, V. Bonache, E. Klyatskina, I. Santacruz, R. Moreno, Preparation and spray drying of Al_2O_3-TiO_2 nanoparticle suspensions to obtain nanostructured coatings by APS, Surface and Coatings Technology 205 (2010) 987-992.
26. K. Masters, Spray drying handbook. 3rd ed. London: George Godwin, 1979.
27. E. Sánchez, J. García-Ten, A. Barba, V. Beltrán, Estimation of packing density of raw material mixtures used in tile manufacture. British Ceramic Transactions and Journal 97 (1998) 149-154.
28. A.W. Jenike, J.R. Johanson, Review of the principles of flow of bulk solids, CIM Transactions 73 (1970) 141-146.
29. X.Y. Wang, Z. Liu, H. Liao, D. Klein, C. Coddet, Microstructure and electrical properties of plasma sprayed porous TiO_2 coatings containing anatase, Thin Solid Films 451-452 (2004) 37-42.

30. M. Vicent, E. Sánchez, A. Moreno, R. Moreno, Preparation of high solids content nano-titania suspensions to obtain spray-dried nanostructured powders for atmospheric plasma spraying, Journal of the European Ceramic Society 32 (2012) 185-194.
31. R.S. Lima, B.R. Marple, From APS to HVOF spraying of conventional and nanostructured titania feedstock powders: a study on the enhancement of the mechanical properties, Surface and Coatings Technology 200 (2006) 3428-3437.
32. D.H.A. Hanaor, C.C. Sorell, Review of the anatase to rutile phase transformation, Journal of Materials Science 46 (2011) 855-874.
33. H. Podlesak, L. Pawlowski, J. Laureyns, R. Jaworski, T. Lampke, Advanced microstructural study of suspension plasma sprayed titanium oxide coatings, Surface and Coatings Technology 202 (2008) 3723-3731.
34. F.L. Toma, G. Bertrand, D. Klein, C. Meunier, S. Begin, Development of photocatalytic active TiO_2 surfaces by thermal spraying of nanopowders, Journal of Nanomaterials (2008), article ID 384171.
35. S. Kozerski, F.L. Toma, L. Pawlowski, B. Leupolt, L. Latka, L.M. Berger, Suspension plasma sprayed TiO_2 coatings using different injectors and their photocatalytic properties, Surface and Coatings Technology 205 (2010) 980-986.
36. B. Ohtani, Preparing articles on photocatalysis − beyond the illusions, misconceptions, and speculation, Chemistry Letters 37 (2008) 217-229.
37. F.L. Toma, G. Bertrand, S. Begin, C. Meunier, O. Barres, D. Klein, C. Coddet, Microstructure and environmental functionalities of TiO_2-supported photocatalysts obtained by suspension plasma spraying, Applied Catalysis B-Environmental 68 (2006) 74-84.
38. H. Chen, S. W. Lee, T. H. Kim, B. Y. Hur, Photocatalytic decomposition of benzene with plasma sprayed TiO_2-based coatings on foamed aluminium, Journal of the European Ceramic Society 26 (2006) 2231-2239.